PIEZO-FIBER COMPOSITES FOR FLUTTER PREDICTION

Flávio D. Marques, fmarques@sc.usp.br
Mateus C. C. Z. Oliveira, mateus.oliveira@usp.br
Volnei Tita, voltita@sc.usp.br
Laboratory of Aeroelasticity, Engineering School of São Carlos – University of São Paulo, São Carlos, SP, Brazil

Mariano E. Moreno, mmoreno@ufscar.br
Federal University of São Carlos, Center of Exact Sciences and Technology, São Carlos, SP, Brazil

Abstract. *Flutter prediction can be improved by understanding the modal coupling mechanism that leads to the instability. However, for complex aeronautical structures, aeroelastic modes identification requires great deal of effort. The use of new types of sensors can improve the flutter prediction assessment. Smart structures technology provides the adequate support for the development of novel sensing approach, for instance, by using the concept of piezo-fiber composites (PFC). This work presents an investigation on the application of piezo-fiber composites to flutter prediction. Here, the PFC is accomplished by assuming piezoelectric ceramic strips bonded to a composite laminate. The finite element method is used to model the piezo-fiber composite, considering an appropriate refined mesh to accomplish meso-micro material behavior. Further steps comprises the use of homogenized properties to achieve a reduced PFC element to incorporate in the aeroelastic modeling. The aeroelastic model comprises coupling a finite element structural model in modal coordinates with an aerodynamic model via unsteady vortex lattice method. By simulating the aeroelastic model, flutter mechanism can be observed from individual modal responses in time and frequency, by changing freestream velocity. Therefore, sensor response can also be assessed and its frequency contents extracted and analyzed. The importance of piezo-fiber composite sensor is analyzed and discussed, thereby providing a promising framework to capture the flutter mechanism and prediction.*

Keywords: *Aeroelasticity, flutter, piezo-fiber composites, active fiber composites.*

1. INTRODUCTION

Flutter prediction of complex aircraft configurations can be improved by understanding its modal coupling mechanism. However, aeroelastic modes identification, particularly in flight, may require great deal of effort. Dedicated sensors could help flutter prediction, speeding up general flight testing or wind tunnel experiments. Novel approaches, such as those related to the smart structures technology provide adequate framework for the development of aeroelastic testing. Actually, with the new technology allowed by smart materials and structures, research in aeroelasticity has gained in strength. The use of new types of sensors and actuators may lead to huge impact on the design of new generations of aerospace vehicles (Friedmann, 1997; Breitbach, 1997). The integration of new smart materials in aeroelasticity provides a challenge in creativity and economy.

More recently, active fiber composites – AFCs (Muller, 2006), made from piezoelectric material fibers embedded in composites, represent a major technological breakthrough for the manufacture of aerospace intelligent structures. The pioneering work on such piezo-fiber composite was by Bent and Hagood (1997). They have manufactured cylindrical piezo-fibers, individually extruded, that were involved in a layer of epoxy resin and installed between two layers of electrodes. The electrodes are used to polarize and to guide the electric field along the polarized piezoelectric fibers. These authors have shown that high actuation energy can be obtained when comparing the performances on d_{33} deformation (deformation in direction 3 with field applied in direction 3) of piezoelectric fibers with the performance in d_{31} (deformation in direction 3 with field applied in direction 1) of monolithic piezoelectric ceramics.

The use of AFCs has been explored by various authors. Generally, these actuators have been used to reduce vibrations on blades of helicopters and for aeroelastic tailoring (Wilkie *et al.*, 1998; Shin *et al.*, 2000; Cesnik *et al.*, 2000). Brown *et al.* (1999) has presented a numerical model of piezoelectric fiber embedded in a composite wing. The results have shown the applicability of these actuators to change the geometry of soft wing, allowing the elimination of articulated flight control surfaces to control rolling motion of unmanned aerial vehicles (UAVs). Moreover, it is also shown the expansion of aircraft flight envelop, exploring the effects of performance in a flexible structure in aeroelastic behavior with piezoelectric fibers.

Using in the reverse way, AFCs become suitable sensors for producing electrical signals needed to close an active control loop, or to apply to identification. Because of AFCs can be built in arbitrary shapes and be embedded in the structures in small intrusive form, there is a great opportunity to use them as modal sensors. The modal sensing must be understood as a method of use of sensors to appropriately acquire vibratory natural modes of structures. Therefore, modal sensors could be used to directly relate the measurements with the structural modes, thereby helping the employment of reduced-order models of complex structures and the development of methods for identification in terms of modes.

Therefore, it is observed here that the use of AFCs as modal sensors is suitable for flutter identification.

Nonetheless, AFC technology is not totally available for extensive application, for instance, in experimental aeroelasticity. Wilkie *et al.* (2000) present an alternative to lower cost to manufacture piezoelectric fibers, the so-called MFC (macro-fiber composites) by cutting and joining together slender strips directly from piezoelectric plates. The two types of fibers operate and perform similarly, differentiated only because of the costs of manufacturing and shape of their cross sections that is cylindrical to AFC and square to MFC.

The objective of this work is to present an investigation on the application of piezo-fiber composites (PFC) to flutter prediction. As a preliminary approach, this study will show a simplified PFC model representing similar idea from AFC and MFC technologies. The finite element method is used to model the piezo-fiber composite, considering an appropriate refined mesh to accomplish meso-micro material behavior. Here, the piezo-fiber is assumed with rectangular cross-section, similarly to the MFC approach, bonded to a composite laminate. To achieve compatible computational performance, the model is reduced to a plate-like finite element by homogenizing the properties from the refined PFC model. Such reduced PFC model is incorporated to the aeroelastic model, in order to proceed on time simulations of a wing aeroelastic response towards flutter instability. The aeroelastic model comprises coupling a structural model with an aerodynamic model via unsteady vortex lattice method, prepared achieve time solutions of modal coordinates. By simulating the aeroelastic model, flutter mechanism can be observed from individual modal responses in time and frequency, by changing freestream velocities. Therefore, sensor response can also be assessed and the frequency contents extracted and analyzed. The PFC sensor performance in capturing the flutter mechanism is analyzed and discussed. Its capabilities for fast predictions on aeroelastic modal variations until coalescence of dominant modes for flutter can be easily highlighted from frequency domain evolutions with respect to freestream velocity. This preliminary study opens reasonable possibilities in efficient and reliable flutter prediction for in-flight and wind tunnel testings.

2. PIEZO-FIBER COMPOSITE FINITE ELEMENT

Piezo-fiber composite (PFC) finite element model has been developed to include to the aeroelastic model. The piezo-composite is detailed in terms of a plate laminate with bonded strips of PZTs. Figure 1 shows illustrations of the global PFC geometry, arrangement, and detailed components. The commercial software ANSYS® has been used to achieve the refined finite element model. To avoid excessive computational effort, the PFC model is reduced to a plate-like equivalent finite element model by adopting an homogenization of the properties from the refined finite element model.

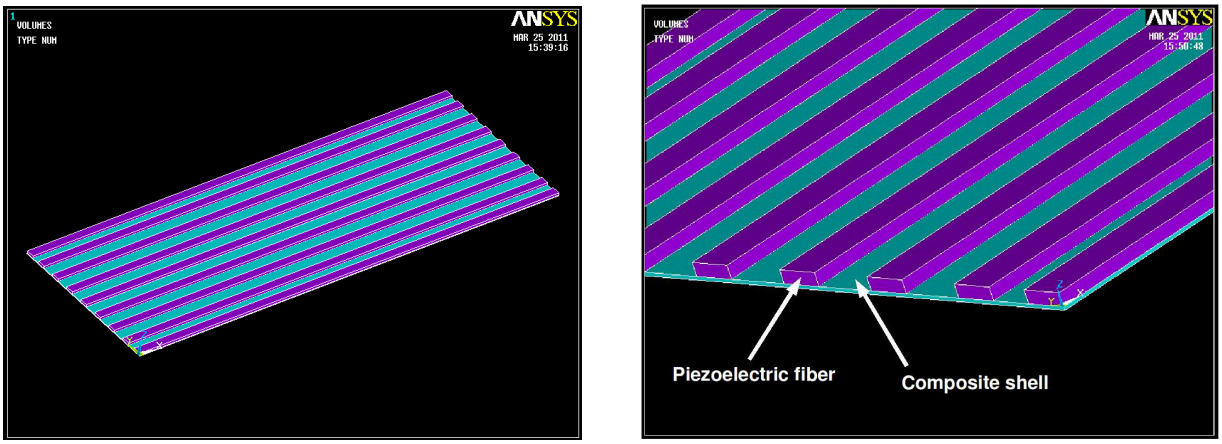

(a) PFC model. (b) Details.

Figure 1. Piezo-fiber composite finite element model.

The effective composite properties are written as a constitutive effective matrix, which includes elastic, electric, and piezoelectric coefficients. This effective matrix relates the average values of stress, strain, electric potential and electrical displacements, evaluated at the whole PFC according to:

$$\left\{ \begin{array}{c} \{\bar{T}\} \\ \{\bar{D}\} \end{array} \right\} = \left[\begin{array}{cc} [C]^{\text{eff}} & [e]^{\text{eff}} \\ [e]^{\text{eff}} & -[\epsilon]^{\text{eff}} \end{array} \right] \left\{ \begin{array}{c} \{\bar{S}\} \\ -\{\bar{E}\} \end{array} \right\} \quad , \tag{1}$$

where $\{\bar{T}\}$ is the average stress field, $\{\bar{D}\}$ is the average electrical displacements field, $\{\bar{S}\}$ is the average strain field, $\{\bar{E}\}$ is the average electrical potential field, $[C]$ is the elasticity matrix, $[\epsilon]$ the dielectric matrix, $[e]$ is the piezoelectric matrix, and $(\,)^{\text{eff}}$ denotes effective property.

Expanding the terms in Eq. (1) and applying symmetry conditions for 1-3 composites, the material coefficients matrix

can be written in terms of independent coefficients, that is,

$$\left\{\begin{array}{c}\bar{T}_{11}\\ \bar{T}_{22}\\ \bar{T}_{33}\\ \bar{T}_{12}\\ \bar{T}_{23}\\ \bar{T}_{31}\\ \bar{D}_1\\ \bar{D}_2\\ \bar{D}_3\end{array}\right\} = \left[\begin{array}{ccccccccc} C_{11}^{\text{eff}} & C_{12}^{\text{eff}} & C_{13}^{\text{eff}} & 0 & 0 & 0 & 0 & 0 & e_{13}^{\text{eff}}\\ C_{21}^{\text{eff}} & C_{22}^{\text{eff}} & C_{23}^{\text{eff}} & 0 & 0 & 0 & 0 & 0 & e_{23}^{\text{eff}}\\ C_{31}^{\text{eff}} & C_{23}^{\text{eff}} & C_{33}^{\text{eff}} & 0 & 0 & 0 & 0 & 0 & e_{33}^{\text{eff}}\\ 0 & 0 & 0 & C_{66}^{\text{eff}} & 0 & 0 & 0 & 0 & 0\\ 0 & 0 & 0 & 0 & C_{44}^{\text{eff}} & 0 & 0 & e_{15}^{\text{eff}} & 0\\ 0 & 0 & 0 & 0 & 0 & C_{44}^{\text{eff}} & e_{15}^{\text{eff}} & 0 & 0\\ 0 & 0 & 0 & 0 & 0 & e_{15}^{\text{eff}} & -\epsilon_{11}^{\text{eff}} & 0 & 0\\ 0 & 0 & 0 & 0 & e_{15}^{\text{eff}} & 0 & 0 & -\epsilon_{22}^{\text{eff}} & 0\\ e_{13}^{\text{eff}} & e_{23}^{\text{eff}} & e_{33}^{\text{eff}} & 0 & 0 & 0 & 0 & 0 & -\epsilon_{33}^{\text{eff}}\end{array}\right] \left\{\begin{array}{c}\bar{S}_{11}\\ \bar{S}_{22}\\ \bar{S}_{33}\\ \bar{S}_{12}\\ \bar{S}_{23}\\ \bar{S}_{31}\\ -\bar{E}_1\\ -\bar{E}_2\\ -\bar{E}_3\end{array}\right\} \quad . \tag{2}$$

To exemplify the average value computation, consider the case of average stress field assessment, that is,

$$\bar{T}_{ij} = \frac{1}{V}\sum_{n=1}^{nel} T_{ij}^{(n)} V^{(n)} \quad , \tag{3}$$

where nel is the number of elements used in the refined model, $T^{(n)}$ is the average stress field at the n^{th} finite element, $V^{(n)}$ is the volume of the n^{th} element, and V is the total volume of the model.

Any other field component present in Eq. (2), such as D_i, S_{ij} or E_i can have their average value obtained as in Eq. (3), and easily post-processed in a standard finite element software.

3. FLUTTER ANALYSIS IN TIME DOMAIN: THE AEROELASTIC MODEL

This section presents a brief description of the aeroelastic model used during simulation in time. The wing structural response is assumed to be linear and without internal damping. The equation of motion for the structure is

$$[M + M_{PFC}]\{\ddot{x}(t)\} + [K + K_{PFC}]\{x(t)\} = \{L(\{x\}, \{\ddot{x}\}, t)\} \quad , \tag{4}$$

where $[M + M_{PFC}]$ and $[K + K_{PFC}]$ are the mass and stiffness matrices with the respective inclusion of piezo-fiber couplings, and $\{x(t)\}$, $\{\ddot{x}(t)\}$ and $\{L(\{x\}, \{\ddot{x}\}, t)\}$ are the vectors, representing the displacements, accelerations and external mechanical, electric and aerodynamic loadings.

The resulting mode shapes can be arranged in a modal matrix,

$$[\Phi] = [\ \{\varphi_1\} \quad \{\varphi_2\} \quad \{\varphi_3\} \quad \cdots \quad \{\varphi_N\}\ ] \quad , \tag{5}$$

and is used as a coordinate transformation matrix, that is:

$$\{x(t)\} = [\Phi]\{\eta(t)\} = \sum_{r=1}^{N} \psi_r \eta_r(t) \quad , \tag{6}$$

where $\{\eta(t)\}$ represents the structural displacements in a modal domain and can be interpreted as a vector of coefficients which determines the influence of each mode shape in the physical structural response (Meirovitch, 1986).

By using the coordinate transformation in Eq. (4) and pre-multiplying both sides by $[\Phi]^T$, followed by normalizing the eingenvectors, it yields,

$$\{\ddot{\eta}(t)\} + [\omega^2]\{\eta(t)\} = [\Phi]^T\{L(\{x\}, \{\ddot{x}\}, t)\} \quad , \tag{7}$$

where $[\omega^2]$ is a diagonal matrix containing the squared natural frequencies.

In order to simplify the solution of Eq. (7), it is useful to consider only a few natural modes to describe the structural response. In fact, only a few modes are necessary to obtain a solution with good precision.

The unsteady aerodynamic loads model is obtained with the Vortex Lattice Method – VLM (Katz and Plotkin, 1991). The VLM consists of distributing plane vortex singularities over a lifting surface and its wake. The plane vortex singularities satisfy the Laplace equation and when it is combined with the uniform stream incompressible and potential flows around the wing the aerodynamic loading can be calculated. Here, to implement the VLM, the wing has been represented by a lifting surface without thickness and discretized in quadrilateral elements (panels). A vortex ring is associated with each panel, being the leading segment of each vortex ring placed on the panel quarter chord line and its control point placed at the center of the three-quarter chord line. To guarantee that the flow streamlines pass over the lifting surface, it is necessary to satisfy the boundary condition of zero normal velocity on the wing surface. This boundary condition is applied at the control points and it results in the correct values for the vortex singularities (circulation Γ).

The boundary condition in each panel can be expressed as $(\nabla\phi + v_m + v_w) \cdot \{n\} = 0$, where the gradient of the potential velocity ϕ corresponds to the perturbed velocities induced by the wing vortex singularities, v_m corresponds to

the velocity of the wing motion (the freestream velocity relative to the wing plus the velocities of the wing structural deformations), v_w corresponds to the velocities induced by the wake, and n is the normal vector.

The velocity V induced by each straight vortex segment, extending from point 1 to point 2, at an arbitrary point P, obeys the Biot-Savart law, that is:

$$V = \frac{\Gamma}{4\pi}\frac{r_1 \times r_2}{|r_1 \times r_2|^2}(r_1 - r_2)\cdot\left(\frac{r_1}{|r_1|} - \frac{r_2}{|r_2|}\right) \quad , \tag{8}$$

where, r_1 and r_2 are the vectors that define the position of point P in relation to the points 1 and 2.

It is important to note that the value of the circulation Γ is still not known in Eq. (8). So, only the values of the other terms will be calculated. This is done by assuming $\Gamma = 1$. The velocity induced by each vortex ring at a point P is obtained adding the results obtained with Eq. (8) for the four corresponding vortex segments. The velocity is referred as the velocity induced by the vortex ring L on the control point K. Applying the zero normal velocity boundary condition at the control point $K = 1$,

$$(V_{11}\Gamma_1 + V_{12}\Gamma_2 + V_{13}\Gamma_3 + \ldots + V_{1m}\Gamma_m + v_{m1} + v_{w1})\cdot n_1 = 0 \quad , \tag{9}$$

where the circulations in each vortex ring are the unknowns and m is the number of panels used in the wing aerodynamic discretization.

Based on Eq. (9), the so-called influence coefficients ($a_{KL} = V_{KL}\cdot n_k$) can be defined. Re-writing this equation as a function of the influence coefficients for each of the m control points and passing v_m and v_w to the right-hand side (RHS) of the equation, the following linear system is obtained:

$$\begin{bmatrix} a_{11} & a_{12} & \cdots & a_{1m} \\ a_{21} & a_{22} & \cdots & a_{2m} \\ \vdots & \vdots & \ddots & \vdots \\ a_{m1} & a_{m2} & \cdots & a_{mm} \end{bmatrix} \begin{Bmatrix} \Gamma_1 \\ \Gamma_2 \\ \vdots \\ \Gamma_m \end{Bmatrix} = - \begin{Bmatrix} v_{m1} + v_{w1} \\ v_{m2} + v_{w2} \\ \vdots \\ v_{mm} + v_{wm} \end{Bmatrix} \cdot \begin{Bmatrix} n_1 \\ n_2 \\ \vdots \\ n_m \end{Bmatrix} \quad . \tag{10}$$

The evaluation of v_m consists of two steps: 1) the freestream velocity is obtained moving the wing in the aft direction, and 2) the velocities of the structural deformations are obtained solving the equation of motion (Eq. (7)). The velocities induced by the wake (v_w vector) are obtained employing the Biot-Savart law (Eq. (8)). The circulation values of the last vortex rings generated are the same as those of the trailing edge vortex rings, to satisfy the three-dimensional Kutta condition. Thus, at each time interval new vortex rings are generated and the corresponding values of circulation are found. The value of circulation of each wake vortex ring remains the same during all the simulation time. In the present simulation, the wake rollup has not been considered, so the wake is parallel to the freestream velocity plane.

The solution of the linear system given by Eq. (10) provides the circulation values for the wing vortex rings, which is employed for the unsteady aerodynamic loads calculation.

The unsteady Bernoulli equation for each panel is:

$$\frac{p_l - p_u}{\rho} = \frac{V_u^2}{2} - \frac{V_l^2}{2} + \frac{\partial\phi_u}{\partial t} - \frac{\partial\phi_l}{\partial t} \quad , \tag{11}$$

where p is the static pressure and the subscripts u and l refer to the upper and lower sides of the panel.

The last two terms in Eq. (11) refer to the unsteady case. The difference between them is obtained from the definition of circulation (Katz and Plotkin, 1991), that is:

$$\frac{\partial\phi_u}{\partial t} - \frac{\partial\phi_l}{\partial t} = \frac{\partial(\phi_u - \phi_l)}{\partial t} = \frac{\partial\Gamma}{\partial t} = \frac{\Gamma(t) - \Gamma(t-1)}{\Delta t} \quad . \tag{12}$$

If $\partial\Gamma/\partial t = 0$, Eq. (11) is analogous to the classical Bernoulli equation for the steady case, and the first two terms can be determined with the aid of the Kutta-Joukowski theorem, that is:

$$\frac{V_u^2}{2} - \frac{V_l^2}{2} = \frac{V_\infty \Gamma \Delta b cos\alpha}{S} \quad , \tag{13}$$

where V_∞ is the free stream velocity, α is the local angle of attack, Δb is the length of the panel in the spanwise direction and S is the panel area.

Substituting Eqs. (12) and (13) into Eq. (11), the normal force in each panel can be computed and supplied as input to the equation of motion (Eq. (7)). It is important to emphasize that the values of Γ in the above equations are given by $\Gamma_{i,j}$ for the wing leading edge panels, and by $(\Gamma_{i,j} - \Gamma_{i-1,j})$ for the other panels.

4. RESULTS

The wing model considers the main structure as aluminum flat plate with $0.8m$ of semi-span, $0.2m$ chord, and thickness of $0.03m$, clamped in one of its spanwise edges. The PFC equivalent plate element is positioned at $0.134m$ from

the clamped edge and $0,05m$ from trailing edge. The PFC element admits a composite plate ($0/90°$, 2 layers fiber glass laminate) with $0.025 \times 0.0667m$, where 9 equally spaced PZT(5A) strips are bonded (each one with $0.38mm$ thickness) along the largest composite plate dimension (*cf.* Fig. 1).

Effective properties for the PFC finite element model can be observed in Tab. 1, where the remaining properties are set equal to zero (*cf.* Eq. (2)). Effective density has been evaluated as $2805\frac{kg}{m^3}$. These values are used to compound the wing model for modal matrix extraction, thereby allowing time domain analysis from Eq. (7).

Table 1. PFC element effective properties.

mechanical (GPa)	**piezoelectrical** (C/m^2)	**electrical** (F/m)
C_{11}^{eff} = 7.55	e_{13}^{eff} = -2.147	$\epsilon_{11}^{\text{eff}} = 38.664 \times 10^{-9}$
C_{12}^{eff} = 3.75	e_{23}^{eff} = -2.144	$\epsilon_{22}^{\text{eff}} = 159.2 \times 10^{-9}$
C_{13}^{eff} = 3.57	e_{33}^{eff} = 29.908	$\epsilon_{33}^{\text{eff}} = 37.447 \times 10^{-9}$
C_{23}^{eff} = 5.24		
C_{22}^{eff} = 29.41		
C_{33}^{eff} = 31.23		

Both finite element and aerodynamic models meshes present 12 longitudinal and 8 transversal elements. Such simplified discretization has been chosen to avoid long time aeroelastic simulations. Aeroelastic simulations have been performed assuming time sampling of $0.001s$, $5.0°$ angle of attack (AoA) step input excitation, and air density of $1.225\frac{kg}{m^3}$. Moreover, PFC element embedded in the wing structure works strictly as sensor, which implies that no electrical voltage is externally applied to it during simulations. Reduced aeroelastic model in modal coordinates has been assessed from the first five modes, at wind-off condition, that comprehend first bending ($1.2936Hz$), second bending ($8.1688Hz$), first torsion ($10.670Hz$), third bending ($23.543Hz$), and second torsion ($32.796Hz$) modes, respectively.

Figures 2 and 3 depict the wing with PFC-type sensor aeroelastic responses in modal coordinates. Two time histories have been chosen to demonstrate the effects of freestream velocity increment to the appearance of flutter phenomenon.

In the first case as shown in Fig. 2 at freestream velocity of $5.0\frac{m}{s}$, typical aerodynamically damped responses can be observed. Figures 2(a) and 2(b) present, respectively, the modal coordinates time histories and their frequency contents.

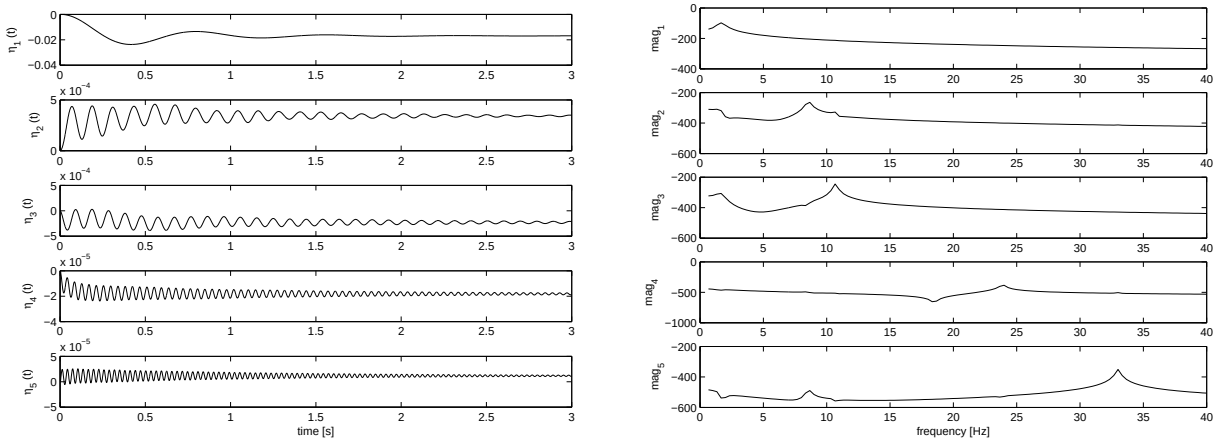

(a) Modal coordinates in time.

(b) Frequency content.

Figure 2. Aeroelastic simulation at $5.0\frac{m}{s}$.

In Fig. 3 the aeroelastic system at $15.0\frac{m}{s}$ reaches flutter condition, clearly observed from modal coordinates increasing amplitudes with time. The exact value of critical flutter speed is hard to be achieved using time simulations, but for the aims of this work, time simulations represent a reasonable framework towards qualifying the PFC-type sensor to predict flutter onset.

Figures 3(a) and 3(b) also help to understand that second bending with first torsion modes are those responsible for the flutter mechanism. Their coalescence provides the dominant frequency that drives the instability to the aeroelastic system. The flutter frequency can be assumed as approximately $9.0Hz$.

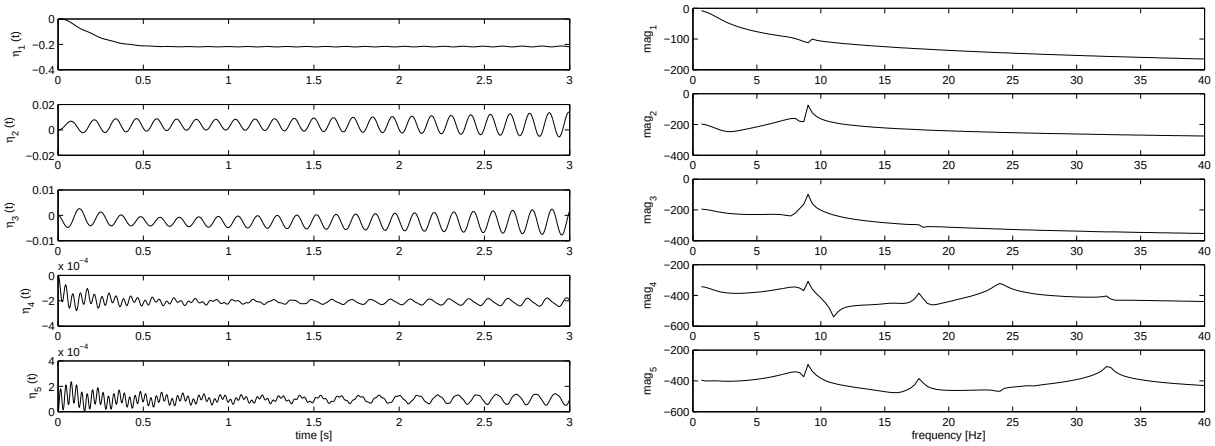

(a) Modal coordinates in time. (b) Frequency content.

Figure 3. Aeroelastic simulation at $15.0\frac{m}{s}$ showing the flutter instability onset.

The results in Figs. 2 and 3 consider only modal coordinates transformation from pure electro-mechanical displacements of the finite element model. The assessment of physical variable values also provides a source of information on aeroelastic evolution towards flutter instability. By following the direct extraction of physical variables, dynamic piezo effect can be captured, thereby assuring the determination of the sensor behavior during flutter prediction.

In Fig. 4 the dynamic behavior of both PFC normalized voltage and angle of attack (AoA) at the wing tip can be observed, as far as their evolutions with freestream velocities are concerned. Either for the PFC sensor or AoA responses provide evident path of flutter onset, although its mechanism lies hidden in the respective time histories. By comparing the PFC sensor with an ideal AoA measurement, one can observe that the PFC keeps more information on the system dynamics, showing more oscillatory components to its response in time. Such feature may be more clearly observed from frequency domain analysis of the PFC signals.

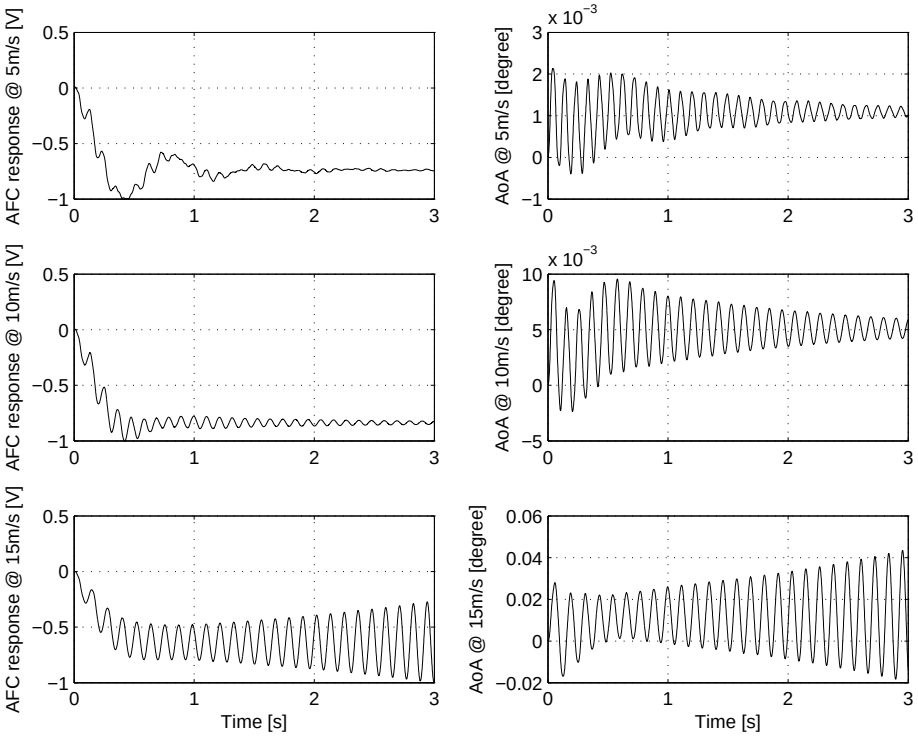

Figure 4. Physical variables time histories evolution with freestream speed – PFC normalized voltage and AoA, respectively.

Figure 5 provides the evolution of PFC sensor responses decomposed in its frequency content with respect to the freestream velocity. This result demonstrates the capability of this kind of sensor to capture the transformations of the aeroelastic system dynamics toward instability. For low speed flowfield, the frequency content shows several components

due to various aeroelastic modes. As the freestream velocity increases the dominance of particular mechanism, in this case driven by first torsion and second bending coupling, is clearly observable. At $10.0\frac{m}{s}$ modes coalescence has already started, which leads to a dominant mode at around $9.0Hz$. Finally, the aeroelastic evolution reveals at $15.0\frac{m}{s}$ the dominance of a low damping mode over the range of former modes of this system, which characteristically indicates the flutter onset.

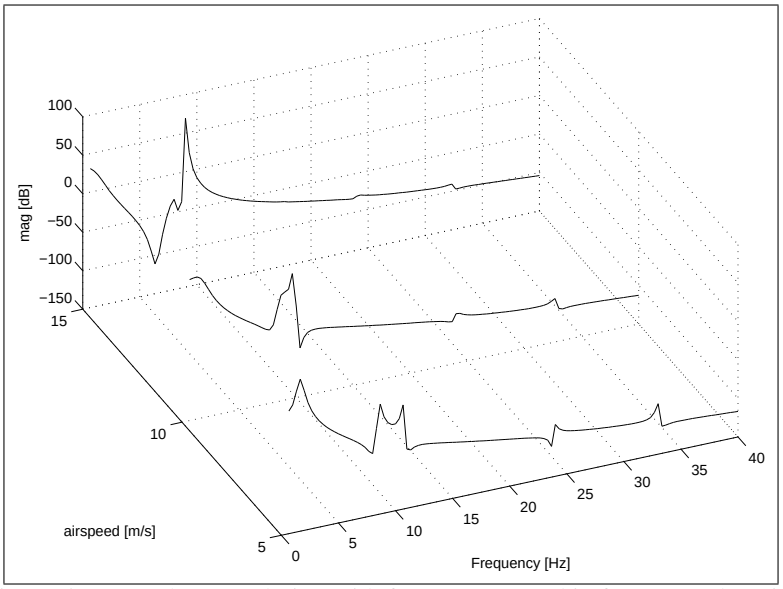

Figure 5. PFC voltage evolution with freestream speed in frequency domain.

5. CONCLUDING REMARKS

This work has presented an investigation on modeling a piezo-fiber composite (PFC) that may improve the flutter prediction for aeroelastic systems. Time domain flutter analysis is considered, where an aeroelastic model in structural modes coordinates is adopted. For aerodynamic loading calculations, the unsteady vortex lattice method is used. PFC-type sensor is modeled using the finite element method and a homogenized PFC element is attained. The need for a reduced version of a PFC element is considered here to improve the computational performance of the aeroelastic simulations. Homogenized features of the PFC sensor is achieved by typical effective properties assessment by averaging a highly discretized finite element model. Aeroelastic simulations have revealed flutter onset at around $15.0\frac{m}{s}$ with frequency of $9.0Hz$. The mechanism of this instability has been also verified from the coalescence of the the second bending with the first torsion modes. The PFC sensor responses alone with freestream velocity show appropriate behavior either in time or frequency domains to help identifying the instability onset, as well as in presenting the frequencies involved during the coupling related to the flutter mechanism. Future work considers extended investigation on PFC sensor with several combinations of composite laminates and PZT strips geometries. The homogenized PFC model shall also be verified to certify that their features remain within a proper operational range. The issue of isolating the flutter mechanism using the PFC sensor will also be considered, as well as using this approach as dedicated modal filtering.

6. ACKNOWLEDGMENTS

The authors are thankful to CAPES, CNPq, and FAPEMIG for funding this present research work through the INCT-EIE.

7. REFERENCES

Bent, A. and Hagood, N., 1997. "Piezoelectric fiber composites with interdigitated electrodes". *Journal of Intelligent Materials Systems and Structures*, Vol. 8, No. 6, pp. 903–911.

Breitbach, E., 1997. "Adaptive structural concepts: State of the art and future outlook". In *Proc. of the Int. Forum on Aeroelasticity and Structural Dynamics, IFASD/CEAS 97*. Roma, Itália,June 17-20, pp. 69–77.

Brown, T., Wood, K., Childers, B., Cano, R., Jensen, B. and Rogowski, R., 1999. "Fiber optic sensors for health monitoring of morphing aircraft". In *Proc. of the SPIE 6^{th} Annual International Symposium on Smart Structures and Materials*. Newport Beach, CA, March 1-5.

Cesnik, C., Ortega-Morales, M. and Patil, M., 2000. "Active aeroelastic tailoring of high aspect ratio composite wings". In *Proc. of the 41^{st} AIAA/ASME/ASCE/AHS/ASC Structures, Structural Dynamics, and Materials Conference*. Atlanta,

Georgia, Apr. 3-6.

Friedmann, P., 1997. "The renaissance of aeroelasticity and its future". In *Proc. of the Int. Forum on Aeroelasticity and Structural Dynamics, IFASD/CEAS 97*. Roma, Itália,June 17-20, pp. 19–49.

Katz, J. and Plotkin, A., 1991. *Low-speed aerodynamics:* from wing theory to panel methods. McGraw-Hill, New York.

Meirovitch, L., 1986. *Elements of Vibration Analysis*. McGraw-Hill, New York.

Muller, M., 2006. "Design of an active fiber composite modal sensor for use in a helicopter rotor blade". Technical report.

Shin, S., Cesnik, C. and Wilbur, M., 2000. "Dynamic response of active twist rotor blades". In *Proc. of the 41st AIAA/ASME/ASCE/AHS/ASC Structures, Structural Dynamics, and Materials Conference*. Atlanta, Georgia, Apr. 3-6.

Wilkie, W., Belvin, W. and Park, K., 1998. "Helicopter dynamic stall suppression using piezoelectric active". In *Proc. of the 39th AIAA/ASME/ASCE/AHS/ASC Structures, Structural Dynamics, and Materials Conference*. Long Beach, CA, Apr. 20-23.

Wilkie, W., Bryant, R., High, J., Fox, R., Hellbaum, R., Jalink, A., Little, B. and Mirick, P., 2000. "Low-cost piezocomposite actuator for structural control applications". In *Proc. of the SPIE 7th Annual International Symposium on Smart Structures and Materials*. Newport Beach, CA, March 5-9.

8. Responsibility notice

The author(s) is (are) the only responsible for the printed material included in this paper